IEEE Access
Multidisciplinary | Rapid Review | Open Access Journal

Date of publication xxxx 00, 0000, date of current version xxxx 00, 0000.

Digital Object Identifier 10.1109/ACCESS.2017.DOI

Rate Compatible Modulation for Non-Orthogonal Multiple Access

IMANOL GRANADA [1], PEDRO M. CRESPO[1], (Senior Member, IEEE), and JAVIER GARCIA-FRÍAS[2], (Senior Member, IEEE)

[1]Department of Biomedical Engineering and Science, Tecnun - University of Navarra, 20018 San Sebastian, Spain
[2]Department of Electrical and Computer Engineering, University of Delaware, Newark, DE 19716 USA

Corresponding author: Imanol Granada (e-mail: igranada@tecnun.es).

This work was supported by the Spanish Ministry of Economy and Competitiveness through the ADELE project (Grant No. PID2019-104958RB-C44). This work has been funded in part by NSF Award CCF-1618653.

ABSTRACT We propose a new Non-Orthogonal Multiple Access (NOMA) coding scheme based on the use of a Rate Compatible Modulation (RCM) encoder for each user. By properly designing the encoders and taking advantage of the additive nature of the Multiple Access Channel (MAC), the joint decoder from the inputs of all the users can be represented by a bipartite graph corresponding to a standard point-to-point RCM structure with certain constraints. Decoding is performed over this bipartite graph utilizing the sum-product algorithm. The proposed scheme allows the simultaneous transmission of a large number of uncorrelated users at high rates, while the decoding complexity is the same as that of standard point-to-point RCM schemes. When Rayleigh fast fading channels are considered, the BER vs SNR performance improves as the number of simultaneous users increases, as a result of the averaging effect.

INDEX TERMS Multiple Access Channel (MAC); Rate Compatible Modulation (RCM); Non-Orthogonal Multiple Access (NOMA); Rayleigh fast fading; Iterative Decoding.

I. INTRODUCTION

ORTHOGONAL Multiple Access (OMA) has been used in past generations of mobile communication systems due to processing limitations or low traffic demands. Orthogonal schemes allow the receiver to separate unwanted signals from the desired ones by utilizing simple strategies. Time Division Multiple Access (TDMA) or Orthogonal Frequency-Division Multiple Access (OFDMA) are two of the most common OMA schemes, where users use their unique assigned time slots or sub-carrier frequency slots, respectively, for communication.

In contrast, in a Non-Orthogonal Multiple Access (NOMA) all users share the same frequency and time intervals for their transmissions. NOMA systems outperform OMA schemes in multiple scenarios, such as downlink systems [1], visible light communication systems [2] and short packet communications [3]. Thus, NOMA plays an important role in 5G [4, 5, 6] and is one of the key technologies that will enable the upcoming 6G networks [7]. NOMA schemes can be divided into two sub-categories [8], namely, power-domain and code-domain NOMA. Power-domain NOMA attains multiplexing by utilizing superposition coding, whereas code-domain NOMA utilizes user-specific spreading sparse sequences or non-orthogonal cross-correlation spreading sequences. This paper primarily focuses on power-domain NOMA.

In NOMA systems, Multi-User (MU) detection algorithms are used to detect the desired signals at the receiver. These detection algorithms can be divided into two major strategies. Successive Interference Cancellation (SIC) techniques exploit differences in signal strength among the signals of interest in order to successively decode information arriving from different users. Starting from the strongest, each signal is decoded by treating the remaining as noise and then subtracting it from the received combined signal. SIC generally requires large differences in the received power of different users. Techniques that make use of SIC are well documented in the literature [9, 10], with recent research in this field focusing specifically on resource allocation. For example, authors in [11] optimize the power allocation in wireless powered communication networks to satisfy the minimum data requirements for each user. In [12] they also studied the optimal power allocation coefficients from a user fairness perspective.

A major disadvantage of SIC is that it suffers from a trade-off between performance gain and implementation complex-

ity [8], since the decoding complexity increases with the number of users involved in the scheme. On the other hand, non-SIC NOMA systems capable of jointly decoding the multiple users have recently experienced a rise in popularity. For example, authors in [13] show that non-SIC NOMA is more effective than traditional SIC NOMA for sending correlated information sources. A novel non-SIC NOMA architecture for near power-balanced scenarios, named Network-Coded Multiple Access, was proposed in [14]. By jointly using physical-layer network coding and multi-user decoding, it is possible to boost NOMA throughputs in power-balanced scenarios, where SIC does not work well. Similarly, [15] combines Bit-Interleaved Coded Modulation (BICM) with Iterative Demapping (ID) and decoding for Multi-User (MU) detection to create MU-BICM-ID systems, which achieve any point on the upper boundary of the MAC capacity region at high rates. However, previous examples in [14, 15] are limited to 3 and 2 users, respectively, since the complexity also increases substantially with the number of users.

An alternative Multiple Access (MA) method, named Interleave Division Multiple Access (IDMA), was proposed in [16] as an alternative to NOMA. IDMA is a an evolution of Code-Division Multiple Access (CDMA) that relies on interleaving as the only means to distinguish signals and employs parallel interference cancellation to detect the multiple users, inheriting many of the advantages provided by Code-Division Multiple Access (CDMA). Authors in [16] accommodate up to 100 users using IDMA. They are also able to achieve high power efficiency, with a BER performance 1.4 dB away from the theoretical limit for a 16-user case and a total throughput of 2 bits per channel use. They do so by utilizing complex Turbo-Hadamard codes. Later, authors in [17] proposed the use of low-rate layered LDGM as the core codes of IDMA schemes, simplifying the structure and allowing the sum-product algorithm to be applied for decoding. The scheme presented in [17] outperforms [16] by achieving a gap to the theoretical limit of 1.05 dB for the same total throughput. This is achieved for 20 users with an individual rate of 0.05. In order to accommodate more users, authors in [17] lowered the individual rates, upper bounding the total throughput to 2 bits per channel use. The gap to the the theoretical limit increases with the number of users, regardless of whether the codes have been optimized for the considered number of users. A comparison between IDMA and NOMA when a channel estimator is used was presented in [18]. Authors show that IDMA outperforms NOMA in power-balanced scenarios at the cost of higher complexity, whereas NOMA outperforms IDMA in power imbalanced scenarios. However, they only considered SIC NOMA, which, as mentioned before, is outperformed by non-SIC NOMA in power-balanced scenarios. To the best of our knowledge, there are no examples in the literature of coding schemes for non-SIC power-balanced NOMA suitable for operating at high spectral efficiency and large number of MAC users. The research of such coding schemes is pivotal to satisfy the ever increasing connectivity and throughput demands of modern wireless networks.

The main contribution of this paper is the proposal of a novel coding technique for the MAC that allows the transmission of multiple users at high rates while guaranteeing that the complexity and the performance is not negatively affected by the number of simultaneous users. The proposed scheme is based on Rate Compatible Modulation (RCM). RCM is a high spectral efficiency coding scheme proposed in [19, 20] for point-to-point communications. These codes are able to naturally perform joint source-channel coding for non-uniform memoryless sources, while achieving seamless and blind rate adaptation. The key idea is to generate multi-level coded symbols from a binary source through weighted linear combinations of the input bits, and to achieve rate adaption by adjusting the number of generated symbols. At the receiver, joint decoding is performed based on the received symbols. Low complexity decoding algorithms have been recently presented in [21], where the performance is only degraded by 0.3 dB when compared to the original decoding algorithm presented in [19]. As illustrated in [20], these schemes outperform conventional Adaptive Code Modulation (ACM), as they are able to overcome the stair-shaped rate curves that characterize standard ACM due to the limited set of rate combinations. RCM schemes can also be used in parallel with Low Density Generator Matrix (LDGM) codes [22, 23, 24, 25], thus overcoming the intrinsic error floor encountered in RCM codes for high Signal to Noise Ratios (SNRs).

The coding scheme proposed in this paper, which we call RCM-MAC, is based on a modified version of point-to-point RCM codes. The idea is to generate weighted linear combinations of each user's own information bits. These linear mappings are constructed in such a manner that the overall superimposed coded symbols at the output of the MAC possess the same structure as a point-to-point RCM code. Therefore, RCM-MAC structures are jointly decoded as point-to-point RCM codes, making the decoding complexity independent of the number of users. RCM-MAC codes inherit the smooth rate adaptability and high spectral efficiency found in point-to-point RCM codes, with performance at a given (high) sum-rate equivalent to that of a point-to-point RCM scheme with a rate equal to the value of the sum-rate.

The remainder of the manuscript is organized as follows. Section II introduces the system model and provides an overview of standard RCM. Two different multiple access channels are considered: the AWGN channel and the Rayleigh fast fading channel. The RCM-MAC code construction is presented in section III, while the decoding process is developed in section IV. The system performance for both models is analyzed in section V. Finally, section VI concludes the paper.

II. BACKGROUND AND SYSTEM MODEL

We begin this section by describing the two communication models considered in this paper, the AWGN multiple access channel and the Rayleigh fast fading multiple access channel.

This article has been accepted for publication in a future issue of this journal, but has not been fully edited. Content may change prior to final publication. Citation information: DOI 10.1109/ACCESS.2020.3043529, IEEE Access

For the reader's convenience, we also provide an overview of Rate Compatible Modulation (RCM) for point-to-point communications.

A. AWGN MULTIPLE ACCESS CHANNEL

Figure 1 shows the system model for the multi-user MAC with λ users over the complex AWGN channel. It is assumed that the information sent by each user is modeled by uniform independent memoryless binary sources. At the transmitters, the binary symbols generated by each user are input to the encoders ε_l, with $l = 1, \ldots, \lambda$, and modulated using QAM before being transmitted over a single-carrier transmission scheme. Although not considered in this paper, other modulation schemes such as OFDM could also be used.

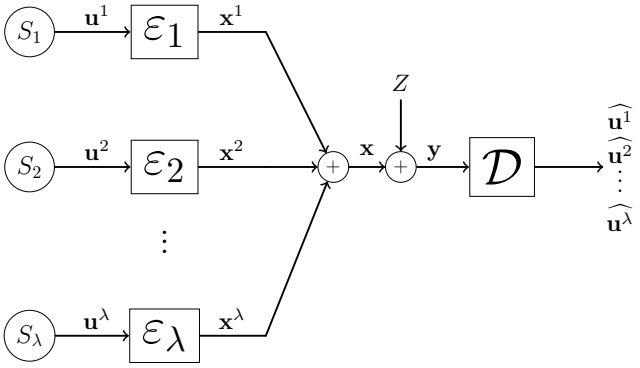

FIGURE 1: The additive white Gaussian multiple access channel considered in this paper.

If we denote the complex baseband sequence at the output of each transmitter as $\mathbf{x}^l$, $l = 1, \ldots, \lambda$, the output of the channel at time j is given by $y_j = \sum_{l=1}^{\lambda} x_j^{(l)} + Z_j$, where the noise components $\{Z_j\}$ are modeled as iid circularly symmetric complex noise random variables with distribution $Z \sim \mathcal{CN}(0, N_0)$. The total transmitted average energy per complex channel use is $E_s = \sum_{l=1}^{\lambda} E_l$, where E_l is the average energy of user l.

The capacity region for the λ-user MAC is given by the set of rate tuples [26] such that

$$\sum_{l \in \mathcal{L}} R_l \leq \log_2 \left(1 + \frac{\sum_{l \in \mathcal{L}} E_l}{N_0}\right), \quad \text{for every} \mathcal{L} \subseteq [1 : \lambda], \tag{1}$$

where R_l is the rate of user l. As we will see later, in this paper the theoretical limit will be imposed by the sum-rate equation

$$R = \sum_{l=1}^{\lambda} R_l \leq \log_2 \left(1 + \frac{\sum_{l=1}^{\lambda} E_l}{N_0}\right) = \log_2 \left(1 + \frac{E_s}{N_0}\right). \tag{2}$$

B. RAYLEIGH FAST FADING MULTIPLE ACCESS CHANNEL

Figure 2 shows the system model for the Rayleigh fast fading multiple access channel with λ independent users. Note that the previous AWGN MAC model is a particular case of the Rayleigh fast fading multiple access model without the fading components $h^{(l)}$, for $l = 1, \ldots, \lambda$.

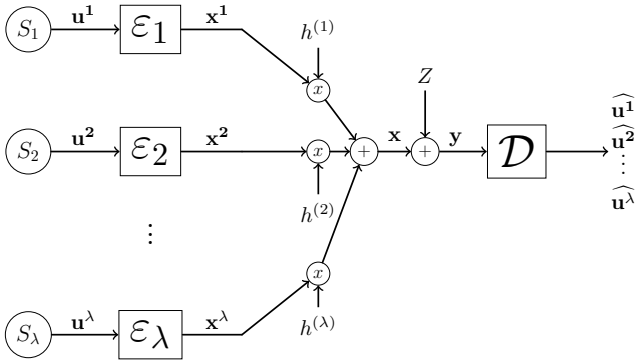

FIGURE 2: The Rayleigh fast fading AWGN multiple access channel considered in this paper.

If we denote the complex baseband sequence at the output of each transmitter as $\mathbf{x}^l$, $l = 1, \ldots, \lambda$, the output of the channel at time j is given by $y_j = \sum_{l=1}^{\lambda} x_j^{(l)} \cdot h_j^{(l)} + Z_j$, where the fading factors $\{h_j^{(l)}\}$ are modeled as iid complex circularly symmetric Gaussian random variables with distribution $h^{(l)} \sim \mathcal{CN}(0, 1)$. Note that in this case the achievable rate bounds are obtained by averaging the inequalities (1) with respect to the exponential random variables $|h^{(l)}|^2 \sim e^{-h}$, $l = 1, \ldots, \lambda$, that is,

$$\sum_{l \in \mathcal{L}} R_l \leq E\left[\log_2 \left(1 + \frac{\sum_{l \in \mathcal{L}} \left|h^{(l)}\right|^2 E_l}{N_0}\right)\right], \quad \text{for every } \mathcal{L} \subseteq [1 : \lambda], \tag{3}$$

where R_l is the rate of user l. Similar to the AWGN channel case, the theoretical limit will be given as

$$R = \sum_{l=1}^{\lambda} R_l \leq E\left[\log_2 \left(1 + \frac{\sum_{l=1}^{\lambda} \left|h^{(l)}\right|^2 E_l}{N_0}\right)\right]. \tag{4}$$

Applying the Jensen Inequality, it follows that the right-side term in (4) is upper-bounded by the corresponding bound in (2). By the Law of Large Numbers, it is easy to check that the upper-bounds for the MAC AWGN and MAC Rayleigh fast fading channels are the same when the number of users goes to infinity.

C. RATE COMPATIBLE MODULATION (RCM) CODES

Standard point-to-point RCM [19, 20] codes are based on random projections that generate multilevel symbols from weighted linear combinations of the input bits. This process can be represented by a bipartite graph, where the edges

connecting input bits and RCM symbols have associated weights. If $\mathcal{W}$, with $\mathcal{W} \subset \mathbb{N}$ and cardinality d_r, is the design weight multi-set[1] of an RCM code, then, its RCM symbols are generated as the sum of $2 \cdot d_r$ randomly chosen input bits weighted by the values in $\pm\mathcal{W}$.

Let G, with dimension $M \times K$, be the incidence sparse matrix of the RCM graph, where rows represent coded symbols, columns represent input bits and the nonzero entry (j, k) is the weight associated to the edge connecting symbol j with input bit k. RCM encoding is performed as follows. The source information bits are first partitioned into blocks of length K. Let $\mathbf{u}$ be a block of information bits. Then, the j^{th} RCM real symbol is given by

$$[G\mathbf{u}]_j = \sum_{k=1}^{K} g_{j,k} u_k, \qquad j \in 1, \ldots, M, \tag{5}$$

where $[\,\cdot\,]_j$ is the element at row j, $g_{j,k}$ denotes entry (j, k) of matrix G, and the operations are in the real field.

Finally, the transmitted QAM modulated baseband sequence $\mathbf{x}$, of length $\frac{M}{2}$, is

$$\mathbf{x} = ([G\mathbf{u}]_1 + i \cdot [G\mathbf{u}]_2, \ldots, [G\mathbf{u}]_{M-1} + i \cdot [G\mathbf{u}]_M), \tag{6}$$

where i is the imaginary unit.

As explained in [19], standard RCM codes have to satisfy three properties. First, in order to generate a fixed constellation, the matrix G has to be regular in terms of its rows, i.e. each row contains the same number of non-zero entries. Second, it has to be as regular as possible with regard to its columns. Third and finally, the design weight multi-set $\mathcal{W}$ should create diverse symbol values, since the information carried in the symbols is upper bounded by the entropy of these symbols.

III. RCM-MAC SYSTEMS

In this section we present the construction of the proposed scheme for the multi-user scenario, where λ users want to transmit their information binary blocks $\mathbf{u}^l$, for $l = 1, \ldots, \lambda$, over a MAC. The proposed RCM-MAC systems consist of a set of λ irregular RCM codes, with encoding matrices $G^{(l)}$, one for each individual user. By irregular RCM it is meant that the weight values utilized in the sums of each RCM symbol vary. We denote by $\mathcal{W}_j^{(l)}$ the design multi-set of user l and RCM symbol j, which generates RCM symbol $[G^{(l)}\mathbf{u}^{\mathbf{l}}]_j$. These RCM symbols are then superimposed in the MAC as sketched in Fig. 3, where different users are represented by unique colors.

Given the additive nature of the RCMs and the MAC, the superimposed MAC symbols can be considered as having been generated by a standard point-to-point RCM code encoding the compound source bit block $\mathbf{u}^d = [\mathbf{u}^1\ \mathbf{u}^2 \ldots \mathbf{u}^\lambda]$. The j^{th} RCM MAC overall symbol is connected to $\mathbf{u}^d$ by means of the weights in $\{\pm\mathcal{W}_j^{(1)}, \pm\mathcal{W}_j^{(2)}, \ldots, \pm\mathcal{W}_j^{(\lambda)}\}$. The main idea behind the design of RCM-MAC systems is to specifically select the multi-sets of the irregular RCMs to match, after the MAC, a point-to-point RCM with design multi-set $\mathcal{W}$ by forcing $\{\mathcal{W}_j^{(1)}, \mathcal{W}_j^{(2)}, \ldots, \mathcal{W}_j^{(\lambda)}\} = \mathcal{W}$ for all j.

For example, consider a 2-user RCM-MAC system, where users 1 and 2 transmit their source blocks $\mathbf{u^1}$ and $\mathbf{u^2}$ utilizing encoding matrices $G^{(1)}$ and $G^{(2)}$, respectively. Assume the following design multi-sets $W_j^{(1)} = \{1, 2\}$, $W_j^{(2)} = \{1\}$ for j odd and $W_j^{(1)} = \{1\}$, $W_j^{(2)} = \{1, 2\}$ for j even. Therefore, odd RCM symbols generated by user 1 and 2 utilize weights $\{1, -1, 2, -2\}$ and $\{1, -1\}$ and even RCM symbols $\{1, -1\}$ and $\{1, -1, 2, -2\}$, respectively. Note that any superimposed MAC symbol is generated by a weighted linear combination of source bits from both users, with resulting weight values $\{1, -1, 1, -1, 2, -2\}$, and consequently, the proposed RCM-MAC system behaves like a standard point-to-point RCM with design multi-set $\mathcal{W} = \{1, 1, 2\}$ encoding the source block given by $[\mathbf{u^1}\ \mathbf{u^2}]$.

A. GENERATION OF THE RCM-MAC ENCODERS

Let R_l, for $l = 1, \ldots, \lambda$, be the rate at which each user transmits, so that the sum-rate is equal to $R = \sum_{l=1}^{\lambda} R_l$. The number of coded symbols per block, M, is fixed and the information block length for user l, K_l, is adjusted to meet the corresponding R_l.

The first step is to find a weight multi-set $\mathcal{W}$ that i) satisfies the third property mentioned in Section II-C and ii) leads to good performance in a point-to-point communication system with information rate equal to the required sum-rate in the multi-user scenario, i.e., $R = \sum_{l=1}^{\lambda} R_l$. This weight set can be found with the aid of the EXIT chart techniques presented in [19]. Once the weight set $\mathcal{W}$ is selected, for each coded symbol at position j we randomly assign each element of $\mathcal{W}$ to one of the λ multi-sets $\mathcal{W}_j^{(l)}$. The probability of being assigned to the multi-set l is proportional to $\frac{R_l}{R}$, except in some instances in which, as explained in the sequel, the probability is set to 0. Notice that some multi-sets, $\mathcal{W}_j^{(l)}$, may be either left empty or have more than one element.

Next, we detail the construction of encoding matrices $G^{(l)}$, for $l = 1, \ldots, \lambda$, to be assigned to each user.

1) **Step 1: Generation of the intermediate matrices $A^{(l)}$, $l = 1, \ldots, \lambda$.**
Define matrices $A^{(l)}$, $l = 1, \ldots, \lambda$, as all zeros $M \times K_l$ matrices. We begin by constructing the first row of matrices $A^{(l)}$ in two steps.
   - Randomly assign each element of $\mathcal{W}$ to one of the λ multi-sets $\mathcal{W}_1^{(l)}$ with probability $\frac{R_l}{R}$.
   - For $l = 1, \ldots, \lambda$ substitute the $2 \cdot |\mathcal{W}_1^{(l)}|$ zero entries, $a_{1,1}, \ldots, a_{1,2\cdot|\mathcal{W}_1^{(l)}|}$, in the first row of matrix $A^{(l)}$ by the elements of $\pm\mathcal{W}_1^{(l)}$. If the set $\mathcal{W}_1^{(l)}$ is empty, the corresponding row is left with zeros.

[1] A multi-set is a generalization of the concept of a set that, unlike a set, allows multiple instances of the multi-set's elements.

This article has been accepted for publication in a future issue of this journal, but has not been fully edited. Content may change prior to final publication. Citation information: DOI 10.1109/ACCESS.2020.3043529, IEEE Access

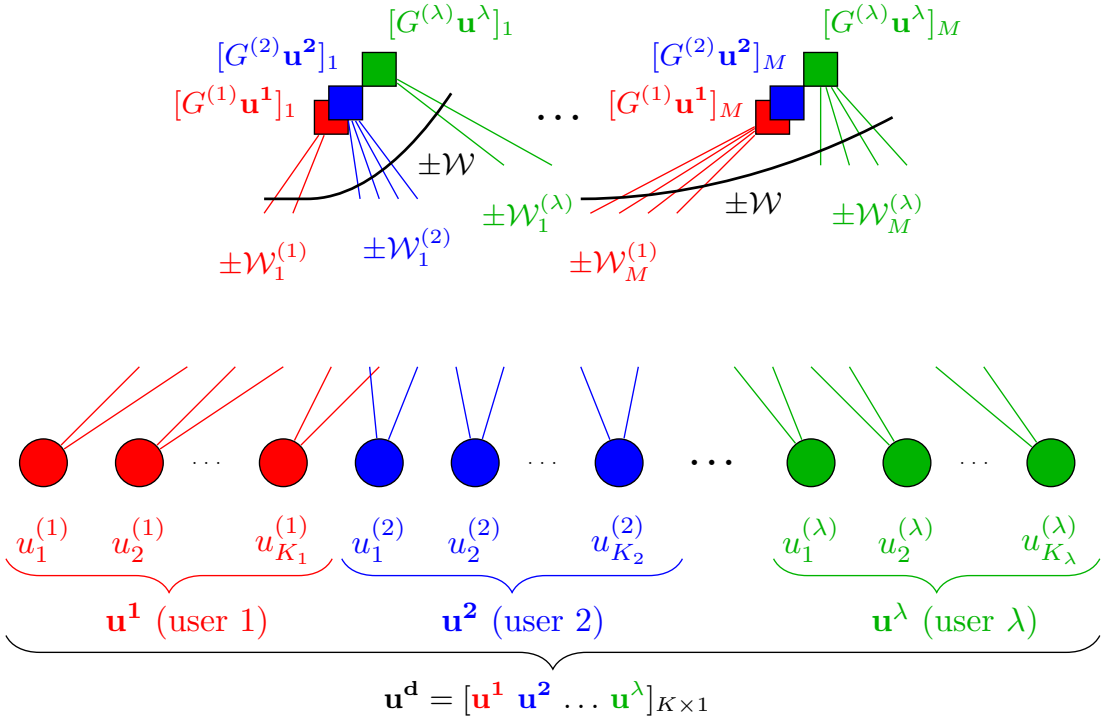

FIGURE 3: Factor graph of the proposed AWGN RCM-MAC scheme with M real coded symbols and λ users, with each user represented by a different color. Each user generates M real coded symbols with an irregular RCM encoder. The j^{th} RCM symbol of user l, $[G^{(l)}\mathbf{u^1}]_j$, is generated from weighted linear combinations of its own source block, of length K_l, utilizing the weight multi-set $\mathcal{W}_j^{(l)}$. Notice that the sum of the λ individual RCM symbols $\{[G^{(1)}\mathbf{u^1}]_j, [G^{(2)}\mathbf{u^2}]_j, \ldots, [G^{(\lambda)}\mathbf{u}^{\lambda}]_j\}$ (performed by the MAC) can be considered as generated by a point-to-point RCM, with weights, $\pm\mathcal{W}$, acting on the compound source bit block $\mathbf{u}^d = [\mathbf{u}^1\ \mathbf{u}^2 \ldots \mathbf{u}^{\lambda}]$ of length $K = \sum_l^{\lambda} K_l$. Notice that by construction $\mathcal{W} = \{\mathcal{W}_j^{(1)}, \mathcal{W}_j^{(2)}, \ldots, \mathcal{W}_j^{(\lambda)}\}$ for $j = 1, \ldots, M$.

Let $\kappa(l)$ be the index of the first column of matrix $A^{(l)}$ whose entries are all zero. Note at this point, $\kappa(l) = 1 + 2 \cdot |\mathcal{W}_1^{(l)}|$ for $l = 1, \ldots, \lambda$.
For $j \geq 2$ until $\kappa(l) > K_l$, $l = 1, \ldots, \lambda$, the row j of matrix $A^{(l)}$ is generated using the following iterative steps:

a) Randomly assign each element of $\mathcal{W}$ to one of the λ multi-sets $\mathcal{W}_j^{(l)}$. The probability of being assigned to the multi-set l is proportional to $\frac{R_l}{R}$, unless $\kappa(l) > K_l$. In this case, the probability of assignment to multi-set $\mathcal{W}_j^{(l)}$ is fixed to 0 (i.e., $\mathcal{W}_j^{(l)}$ will be void), and the remaining probabilities are re-normalized. This is done to promote that the condition $\kappa(l) > K_l$, $l = 1, \ldots, \lambda$, be met for all users in a similar number of iterations, with the goal of obtaining final encoding matrices that are regular in columns.

b) For $l = 1, \ldots, \lambda$ and when $\kappa(l) + 2 \cdot |\mathcal{W}_j^{(l)}| \leq K_l$ substitute the $2 \cdot |\mathcal{W}_j^{(l)}|$ zero entries, $a_{j,\kappa(l)}, \ldots, a_{j,\kappa(l)+2\cdot|\mathcal{W}_j^{(l)}|}$, in row j of matrix $A^{(l)}$ by the elements of $\pm\mathcal{W}_j^{(l)}$. Otherwise, note that there will be $\left(\kappa(l) + 2 \cdot |\mathcal{W}_j^{(l)}| - K_l - 1\right)$ elements that can not be allocated in this manner. These remaining elements are then randomly placed in the unoccupied positions (1 to $\kappa(l) - 1$) of this row[2].

c) Set $\kappa(l) = \kappa(l) + 2 \cdot |\mathcal{W}_j^{(l)}|$, $l = 1, \ldots, \lambda$ and go to the next iteration step with $j = j + 1$.

Denote by J_0 the value of j for which the condition $\kappa(l) > K_l$ is met for all l. Then, matrices $A^{(l)}$, $l = 1, \ldots, \lambda$, are obtained by discarding their last $M - J_0$ zero rows. Note that this construction requires J_0 to be smaller than M. However, the expected value of J_0 is $\frac{K}{2 \cdot d_r}$, independent of the number of users, allowing a potentially unlimited number of simultaneous users.

2) **Step 2: Generation of the encoding matrices $G^{(l)}$,** $l = 1, \ldots, \lambda$. Matrix $G^{(l)}$, is obtained by vertically stacking L randomly column-wise permuted $A^{(l)}$ matrices, where $M \leq LJ_0 < M + J_0$. Note that in the last stacked permuted matrix, $A^{(l)}$, only $V = M - (L-1)J_0$ rows should be kept

The proposed RCM-MAC construction ensures that the superimposed coded symbols at the output of the MAC

[2]It can be assumed that the individual block length of the users is always much larger than the length of weight set $K_l >> 2 \cdot |\mathcal{W}| \geq 2 \cdot |\mathcal{W}_j^{(l)}|$. Therefore, there will always be enough unoccupied positions to place these $\left(\kappa(l) + 2 \cdot |\mathcal{W}_j^{(l)}| - K_l - 1\right)$ elements.

channel are a weighted linear combination of the input bits proceeding from several users, with the weights belonging to $\pm\mathcal{W}$. Considered as a point-to-point RCM code, an RCM-MAC structure satisfies the three properties of good RCM codes, as mentioned in Section II.C: i) it is regular in rows, with a "total" design weight set $\mathcal{W}$ by construction; ii) its weight set creates diverse symbol values which can carry the information of all users; and iii) the constructed encoding matrix is also regular in columns.

Notice that due to the use of symmetric weights $\pm\mathcal{W}_j^{(l)}$, we ensure that the output constellation for each user has zero mean, minimizing the average energy per user. In this work, we only consider uncorrelated users. Thus, coded symbols from different users remain uncorrelated, and, assuming no noise, the mean energy of the MAC output is the sum of the transmitted mean energies of all users. Since some users may not transmit during certain time slots, superposition coding and time division occur implicitly within the proposed RCM-MAC scheme, especially when the number of users increases.

IV. RCM-MAC DECODER

In this section we present the decoding strategy for RCM-MAC codes. Recall that the objective of the proposed scheme is to create a multi-user coding system that emulates a point-to-point RCM code. With the construction method explained in Section III, the superimposed coded symbols at the output of the MAC channel are weighted combinations of the source bits proceeding from several users, with the weights belonging to $\pm\mathcal{W}$. By jointly considering the information bits of all users, from the decoder's perspective the resulting structure is equivalent to a point-to-point system. Thus, the decoding complexity does not depend on the number of users, and, for the AWGN scenario, the decoder is exactly the same as its point-to-point counterpart.

The decoding strategy for multi-user RCM-MAC codes follows this criteria of considering the entire multi-user communication system as an equivalent point-to-point RCM code. As a general case, which includes the AWGN scenario as a particular case, we begin this section by defining the decoding matrix G^d for the Rayleigh fast fading MAC. Matrix G^d represents the equivalent point-to-point system over which the sum-product algorithm is performed.

A. DECODER FOR THE RAYLEIGH FAST FADING MAC

When perfect Channel State Information (CSI) is available at the receiver in point-to-point communications, the fading complex gain h_j of coded symbol j is canceled by multiplying the received sample by $\frac{\overline{h_j}}{|h_j|^2}$, where $\overline{h_j}$ denotes the conjugate of h_j. Decoding is performed by incorporating the scaling factor $\frac{1}{|h_j|^2}$ to the noise variance of symbol j in the factor graph. However, in the multi-user scenario this is not possible, since the received symbols are combinations of several coded symbols, each with its own fading factor $\{h_j^{(1)}, h_j^{(2)}, \ldots, h_j^{(\lambda)}\}$. In order to decode RCM-MAC systems using standard belief propagation, the fading factors have to be taken into account in the overall factor graph. We begin by rewriting each of the $\frac{M}{2}$ received complex symbols as

$$\begin{aligned} y_j &= \sum_{l=1}^{\lambda} x_j^{(l)} \cdot h_j^{(l)} + Z_j \qquad\qquad \text{for } j = 1, \ldots, \frac{M}{2} \\ &= \sum_{l=1}^{\lambda} \Big(\underbrace{\sum_{k=1}^{K_l} g_{2j-1,k}^{(l)} u_k^{(l)}}_{[G^{(l)}\mathbf{u^1}]_{2j-1}} + i \cdot \underbrace{\sum_{k=1}^{K_l} g_{2j,k}^{(l)} u_k^{(l)}}_{[G^{(l)}\mathbf{u^1}]_{2j}} \Big) \cdot h_j^{(l)} + Z_j \\ &= \sum_{l=1}^{\lambda} \left(\sum_{k=1}^{K_l} \left(\left(g_{2j-1,k}^{(l)} + i \cdot g_{2j,k}^{(l)} \right) \cdot u_k^{(l)} \cdot h_j^{(l)} \right) \right) + Z_j, \end{aligned} \tag{7}$$

where K_l is the block length of user l and i is the imaginary unit. The term $g_{j,k}^{(l)}$ belongs to the entry (j,k) of the sparse encoding matrix $G^{(l)}$ and $h_j^{(l)}$ is the complex fading factor for the complex symbol j of user l.

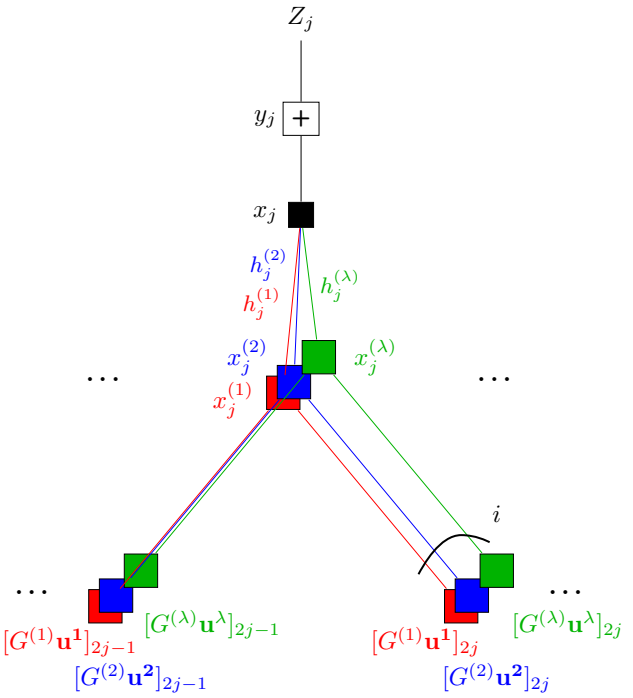

FIGURE 4: Factor graph of the j^{th} received MAC symbol y_j based on (7). The QAM modulated transmitted RCM symbols $[x_j^{(1)}, x_j^{(2)}, \ldots, x_j^{(\lambda)}]$, obtained as $x_j^{(l)} = \left([G^{(l)}\mathbf{u^1}]_{2j-1} + i \cdot [G^{(l)}\mathbf{u^1}]_{2j} \right)$ for $l = 1, \ldots, \lambda$, are multiplied in the MAC by the complex fading factors $[h_j^{(1)}, h_j^{(2)}, \ldots, h_j^{(\lambda)}]$ before being added together.

Figure 4 illustrates the complex factor graph of the j^{th} received MAC symbol for the λ-user RCM-MAC system based on (7). Starting from the bottom, the real RCM symbols $[G^{(l)}\mathbf{u^1}]_{2j-1}$ and $[G^{(l)}\mathbf{u^1}]_{2j}$, for $l = 1, \ldots, \lambda$, are obtained as in Fig. 3. These RCM real symbols are then

paired two-by-two into the transmitted RCM QAM symbols $x_j^{(l)} = \left([G^{(l)}\mathbf{u^l}]_{2j-1} + i \cdot [G^{(l)}\mathbf{u^l}]_{2j}\right)$. Following this, each of these transmitted RCM QAM symbols is multiplied by its own complex fading factor $h_j^{(l)}$, making it impossible for the receiver to cancel the fading factors, as is usually done in point-to-point fading channels. These complex multiplications mix the real (in-phase) and imaginary (quadrature) part of the signals. In order to avoid the creation of cycles of degree 4 that arise when separating the real and imaginary parts, we perform decoding over the two-by-two complex modulated fading factor graph, defining the decoding matrix G^d as

$$G^d = \left[H^{(1)} \cdot \widetilde{G}^{(1)} \quad H^{(2)} \cdot \widetilde{G}^{(2)} \quad \dots \quad H^{(\lambda)} \cdot \widetilde{G}^{(\lambda)}\right]_{\frac{M}{2} \times K}, \tag{8}$$

where $H^{(l)}$, for $l = 1, \dots, \lambda$, is a complex diagonal matrix, of size $\frac{M}{2} \times \frac{M}{2}$, whose diagonal elements are the channel complex fading factors $[h_1^{(l)} h_2^{(l)} \dots h_{\frac{M}{2}}^{(l)}]$. The matrices $\widetilde{G}^{(l)}$, of size $\frac{M}{2} \times K$, are obtained from the matrices $G^{(l)}$ as follows. Each row j, for $j = 1, \dots, \frac{M}{2}$, of $\widetilde{G}^{(l)}$ is obtained by adding the $2j-1$ row in $G^{(l)}$ and the $2j$ row in $G^{(l)}$ multiplied by the imaginary unit i, as in the illustration of Fig. 4. From the receiver's perspective, the output of the fading MAC can be seen as a point-to-point RCM with varying weight multi-sets, which change due to the effect of the fading factors.

Finally, the receiver can decode the extended block $\mathbf{u^d}$ of length $K = \sum_{l=1}^{\lambda} K_l$, defined as $[\mathbf{u}^1\ \mathbf{u}^2\ \dots\ \mathbf{u}^\lambda]$, by executing the sum-product algorithm [27] over the graph describing (8) (refer to Section IV-C). Notice that with this definition of G^d, the received MAC complex RCM sequence $\mathbf{x}$ can be considered as an RCM coded sequence generated by the irregular point-to-point RCM defined by G^d, i.e. $\mathbf{x} = G^d\mathbf{u}^d$.

B. DECODER FOR THE AWGN MAC

The decoder for the AWGN MAC can be seen as a particularization of the Rayleigh fast fading case, where the fading matrices $H^{(l)}$, for $l = 1, \dots, \lambda$, are the $\frac{M}{2} \times \frac{M}{2}$ identity matrix $I_{\frac{M}{2}}$. Thus, in this case, the equivalent decoding matrix G^d can be defined as

$$G^d = \left[\widetilde{G}^{(1)} \quad \widetilde{G}^{(2)} \quad \dots \quad \widetilde{G}^{(\lambda)}\right]_{\frac{M}{2} \times K}, \tag{9}$$

where the matrices $\widetilde{G}^{(l)}$, for $l = 1, \dots, \lambda$, are defined as in Section IV-A. In the AWGN MAC scenario, the combined symbols at the output of the MAC are treated as standard RCM symbols, with corresponding multi-set $\mathcal{W}$. Note that the generated matrix G^d of size $\frac{M}{2} \times K$ has the same design parameters as a standard point-to-point RCM code but with some additional structure, produced by the constrained positions in which the weights are placed.

C. SUM-PRODUCT ALGORITHM FOR RCM-MAC

In this section we present the details of the sum-product algorithm applied to the complex fading factor graphs defined by G^d in Sections IV-A and IV-B for Rayleigh fast fading and AWGN MAC, respectively. In both cases, since complex channel symbols are considered, the number of check nodes is $\frac{M}{2}$ instead of M.

Let $r_{j,k}$ and $q_{k,j}$ denote the Log-Likelihood Ratio (LLR) messages passed from the j^{th} complex MAC-Check Node (MAC-CN T_j) to the k^{th} Variable Node (VN U_k^d) of $\mathbf{u^d}$, and from the k^{th} VN to the j^{th} complex MAC-CN, respectively. In what follows, we denote by $n(U_k^d) \setminus T_j$ and $n(T_j) \setminus U_k^d$ the set of MAC-CNs connected to VN U_k^d without considering MAC-CN T_j, and the set of VNs connected to MAC-CN T_j without considering VN k, respectively.

At each iteration t, the sum-product algorithm is implemented by the sequential execution of the following steps:

- **STEP 1. $q_{k,j}^{(t)}$: Message passing from variable nodes, $\{U_k^d\}_{k=1}^K$, to MAC-check node $\{T_j\}_{j=1}^{\frac{M}{2}}$.**

$$q_{k,j}^{(t)} = \sum_{i \in n(U_k^d) \setminus T_j} r_{i,k}^{(t-1)}, \tag{10}$$

  where $r_{i,k}^{(0)} = 0$ for $k \in \{1, \dots, K\}$, $i \in n(U_k^d) \setminus T_j$.

- **STEP 2. $r_{j,k}^{(t)}$: Message passing from MAC-check node, $\{T_j\}_{j=1}^{\frac{M}{2}}$, to variable nodes $\{U_k^d\}_{k=1}^K$.**
  Let us define $a_{j,k} = \sum_{i \sim k} g_{j,i}^d u_i^d$, where $\sum_{i \sim k}$ means the sum over all i except k, and rewrite $x_j = \sum_i g_{j,i}^d u_i^d$ as $x_j = a_{j,k} + g_{j,k}^d u_k^d$. Given the received symbol $y_j = x_j + z_j$, $r_{j,k}(t)$ is calculated as

$$r_{j,k}^{(t)} = \log\left(\frac{\sum_s P^{(t)}(a_{j,k} = s) \cdot e^{-\left|y_j - s - g_{j,k}^d\right|^2 / N_0}}{\sum_s P^{(t)}(a_{j,k} = s) \cdot e^{-|y_j - s|^2 / N_0}}\right), \tag{11}$$

  where $|\cdot|$ is the modulus and the sum in s is over all possible values that the MAC-CN RCM symbols can take. Note that $P^{(t)}(a_{j,k} = s)$, the probability of $a_{j,k} = s$ at iteration t, is calculated in a straightforward manner by convolving the probability density functions (PDFs) of the terms in the summation, where the distribution functions of these terms are obtained from the received LLR messages $q_{k,j}^{(t)}$.

When $t = t_{max}$, at the end of the iterations, the estimate of u_k^d is obtained as

$$\widehat{u_k^d} = \begin{cases} 1, & \left(\sum_{i \in n(U_k^d)} r_{i,k}^{(t_{max})}\right) > 0 \\ 0, & \text{otherwise.} \end{cases} \tag{12}$$

Finally, the estimates of $\mathbf{u^i}$, for $i = 1, \dots, \lambda$, are obtained from the bit estimates of $\mathbf{u^d}$ of the corresponding positions of the generated concatenation.

D. EXIT CHARTS OF RCM-MAC CODES

The design of the weight multi-sets $\mathcal{W}$ for the proposed RCM-MAC scheme is based on the equivalent point-to-point

This article has been accepted for publication in a future issue of this journal, but has not been fully edited. Content may change prior to final publication. Citation information: DOI 10.1109/ACCESS.2020.3043529, IEEE Access

RCM code, and, therefore, the same design tools as for RCM codes can be used. It should be mentioned that optimal design procedures for RCM codes are not known. The optimization of RCM codes can be seen as a trial and error process, where different degree distributions and weight sets are tested in order to determine the combination that optimizes performance. This can be done by running time-consuming Monte Carlo simulations. In order to speed up the design, avoiding time-consuming simulations, [19] was the first to propose the use of EXIT charts to predict the performance for different combinations of design parameters in RCM codes. EXIT charts are a tool to analyze the asymptotic convergence of iterative decoders and receivers, by visually tracking the bit-wise mutual information of the messages exchanged in the decoder [28]. These bit-wise mutual transfer curves are suboptimal, since they do not consider dependencies between messages produced by cycles always existing in coding structures of finite block length. Moreover, the Probability Density Function (PDF) of the messages passed from the variable nodes to the check nodes are approximated by a single Gaussian distribution [29], leading to optimistic convergence threshold predictions [30]. However, it was shown in [24] that EXIT charts are able to accurately predict the BER vs SNR performance in both AWGN and Rayleigh fast fading channels for point-to-point RCM systems, making them, therefore, appropriate for RCM-MAC codes.

For the AWGN MAC, the EXIT charts of RCM-MAC codes are identical to the EXIT charts of point-to-point RCM codes with rate equal to the MAC sum-rate. Therefore, the EXIT chart analysis developed in [24] can be directly applied for RCM-MAC codes. On the other hand, when the Rayleigh fast fading MAC is considered, the presence of different fading factors multiplying the weights connecting the users makes EXIT curves depend on the number of users and their rate splits. Thus, when obtaining the conditional PDF of the extrinsic LLR message at the Check Node (CN) decoder by Monte Carlo simulation, one has to take into account the fading factors $[h^{(1)}, h^{(2)}, \ldots, h^{(\lambda)}]$ of the λ users. This is different from the point-to-point case in [24], where only one fading term is considered. Finally, the Variable Node (VN) EXIT curve remains the same as in point-to-point RCM codes.

V. RESULTS

To validate the performance of the proposed RCM-MAC schemes, we next present numerical results obtained by Monte Carlo simulations. We have considered three high rate scenarios with sum-rate, R, equal to 6, 7.4 and 9 bits per complex channel symbol. The total number of information bits transmitted per block K is 37000, and the block length of each user has been adjusted according to the number of users and their rate splits. Specifically, we use matrices $\widetilde{G}^{(l)}$ that generate blocks of $\frac{M}{2} = \frac{K}{R}$ complex coded symbols ($\frac{12334}{2}$, $\frac{10000}{2}$ and $\frac{8226}{2}$ for $R = 6$, 7.4 and 9, respectively). At the receiver side, decoding is performed by applying the sum-product algorithm over the factor graph represented by G^d, as explained in Section IV. The computational complexity of the decoder is determined mainly by the convolution operations that are performed at the symbol level on step 2 of the decoding algorithm. Although not considered in this paper, the low complexity approximation decoding techniques proposed in [21] are straightforward to apply for RCM-MAC systems if the practical application utilizes devices with low computational capabilities.

We consider two different rate allocation schemes. We start by studying the case where the λ users transmit with symmetric rate allocation: Each user utilizes blocks of $\frac{37000}{\lambda}$ information bits (or the closest number to 37000 that is divisible by λ). We have also considered the case where the λ users transmit in an asymmetric way, while maintaining a total sum-rate R equal to 6, 7.4 and 9 bits per complex channel symbol. In this case, the source block length of user l with rate R_l is given by the closest integer to $37000\frac{R_l}{R}$. Table 1 summarizes the 7 different asymmetric rate allocations with (a) $\lambda = 2$, (b) $\lambda = 3$, (c) $\lambda = 4$, (d) $\lambda = 5$, (e) $\lambda = 9$, (f) $\lambda = 13$ and (g) $\lambda = 16$ users that are simulated in this paper.

TABLE 1: Rate allocations in bits per complex channel symbol for the asymmetric case considered in this paper.

	λ	R_ls for $R = 6$
a	2	$\{2, 4\}$
b	3	$\{2 \times 1.5, 3\}$
c	4	$\{0.5, 2 \times 1.5, 2.5\}$
d	5	$\{2 \times 0.66, 2 \times 1.33, 2\}$
e	9	$\{4 \times 0.4, 4 \times 0.8, 1.2\}$
f	13	$\{4 \times 0.2, 4 \times 0.4, 4 \times 0.6, 1.2\}$
g	16	$\{4 \times 0.15, 4 \times 0.3, 4 \times 0.45, 4 \times 0.6\}$
	λ	R_ls for $R = 7.4$
a	2	$\{2.46, 4.93\}$
b	3	$\{2 \times 1.85, 3.7\}$
c	4	$\{0.62, 2 \times 1.85, 3.08\}$
d	5	$\{2 \times 0.82, 2 \times 1.64, 2.46\}$
e	9	$\{4 \times 0.49, 4 \times 0.98, 1.48\}$
f	13	$\{4 \times 0.24, 4 \times 0.49, 4 \times 0.74, 1.48\}$
g	16	$\{4 \times 0.185, 4 \times 0.37, 4 \times 0.55, 4 \times 0.74\}$
	λ	R_ls for $R = 9$
a	2	$\{3, 6\}$
b	3	$\{2 \times 2.25, 4.5\}$
c	4	$\{0.75, 2 \times 2.25, 3.75\}$
d	5	$\{2 \times 1, 2 \times 2, 3\}$
e	9	$\{4 \times 0.6, 4 \times 1.2, 1.8\}$
f	13	$\{4 \times 0.3, 4 \times 0.6, 4 \times 0.9, 1.8\}$
g	16	$\{4 \times 0.225, 4 \times 0.45, 4 \times 0.675, 4 \times 0.9\}$

A. POWER ALLOCATION

Due to the construction method explained in Section III, the power allocation in the RCM-MAC scheme is proportional to the share of total rate of each user, i.e. $\frac{E_l}{E_s} = \frac{R_l}{R}$ for $l = 1, \ldots, \lambda$. In the AWGN case, it is easy to show that given any

This article has been accepted for publication in a future issue of this journal, but has not been fully edited. Content may change prior to final publication. Citation information: DOI 10.1109/ACCESS.2020.3043529, IEEE Access

set of average energies $\{E_1, \ldots, E_\lambda\}$ with $\sum_{l=1}^{\lambda} E_l = E_s$, the set of rates $\{R_1, \ldots, R_\lambda\}$, $R_l \leq \frac{E_l}{E_s} R^*$ is achievable, where R^* is the theoretical limit for the sum-rate given by (2). Similarly, in the Rayleigh fast fading case, for all the set of rates $\{R_1, \ldots, R_\lambda\}$ considered in this paper, the theoretical limit is also defined by the sum-rate equation given in (4).

Notice that independently of the number of users and the rate allocations, for an AWGN MAC with a fixed E_s, the sum-rate can be achieved not only by superposition as in the RCM-MAC scheme, but also with point-to-point RCM codes combined with an adequate time-division multiple access (TDMA) [26] (provided that users are allowed to use an average mean energy E_s during their transmission periods). However, many practical applications impose mean energy limitations (lower than E_s) on each user, making RCM-MAC the best option in such cases.

On the other hand, when Rayleigh fast fading is considered as the number of users increases, the performance of superposition coding overpasses the performance of a TDMA scheme, even if users are allowed to use higher powers during their transmission times. In other words, the combination of a point-to-point RCM code and a TDMA scheme with power control does not achieve the same performance attained when using superposition coding with an RCM-MAC scheme (refer to Section V-C).

B. NUMERICAL RESULTS FOR AWGN MAC

We begin by analyzing the performance of the proposed RCM-MAC scheme for the AWGN channel. The corresponding theoretical limits given by (2) are SNR $= \frac{Es}{N_0} = 18$ dB for $R = 6$, SNR $= 22.3$ dB for $R = 7.4$ and SNR $= 27.1$ dB for $R = 9$.

Fig. 5 shows the BER versus SNR for the symmetric multi-user scenario, with λ =2, 3, 4, 8, 16, 32, 64 and 128 users, whereas results for the asymmetric rate allocations of Table 1 are shown in Fig. 6. To provide further context, we have also depicted the performance of a standard RCM [19] code with the same rate in a point-to-point AWGN channel. Its performance is equivalent to performing the OMA strategy of TDMA with power control, as discussed previously. The weight sets $\mathcal{W}$ considered in the simulations are $\{3, 3, 4, 5\}$, $\{3, 4, 5, 7\}$ and $\{3, 4, 5, 5, 7\}$ for R =6, 7.4 and 9, respectively. They have been selected using EXIT charts of standard point-to-point RCM codes, with a rate equal to the intended sum-rate R, as explained in Section IV-D. Notice that in all cases the proposed RCM-MAC scheme presents a waterfall around 2 dBs away from the sum-rate capacity limit (2). As the number of users increases, the additional structure that is imposed on the construction of the generation matrices $G^{(l)}$ results in higher error floors compared to the point-to-point code. This degradation of the error floor with the number of users is more pronounced when the sum-rate increases. For example, in the scenario with $R = 9$ and symmetric rate allocation shown in Fig. 5c, the error floor goes from near 10^{-5} for $\lambda = 2$, to 10^{-4} and $7{\cdot}10^{-4}$ for $\lambda = 16$ and $\lambda = 128$, respectively.

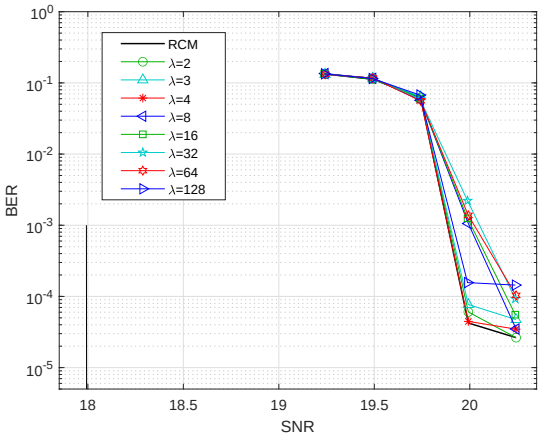

(a) $R = 6$

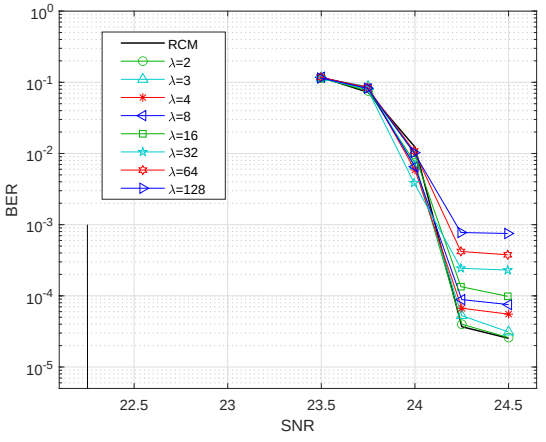

(b) $R = 7.4$

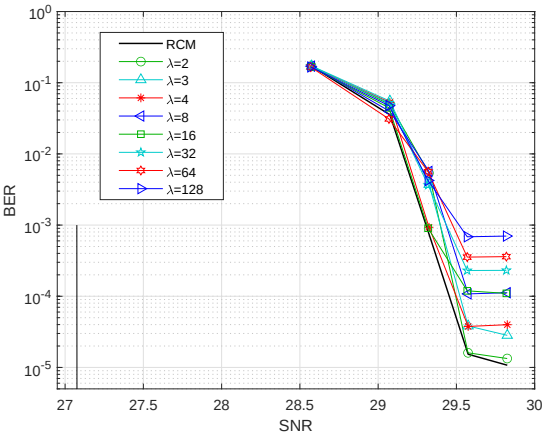

(c) $R = 9$

FIGURE 5: Numerical results obtained by Monte Carlo simulations for the symmetric multi-user scenario with $\lambda \in \{2, 3, 4, 8, 16, 32, 64, 128\}$ users and for point-to-point (RCM) when the AWGN MAC is considered. The weight sets $\mathcal{W}$ are (a) $\{3, 3, 4, 5\}$ for $R = 6$, (b) $\{3, 4, 5, 7\}$ for $R = 7.4$ and (c) $\{3, 4, 5, 5, 7\}$ for $R = 9$.

The increase of the error floor as the number of users increases can be explained by the decrease of the individual block length K_l of each user, which is inversely proportional to the number of users. This effect can be eliminated if the

This article has been accepted for publication in a future issue of this journal, but has not been fully edited. Content may change prior to final publication. Citation information: DOI 10.1109/ACCESS.2020.3043529, IEEE Access

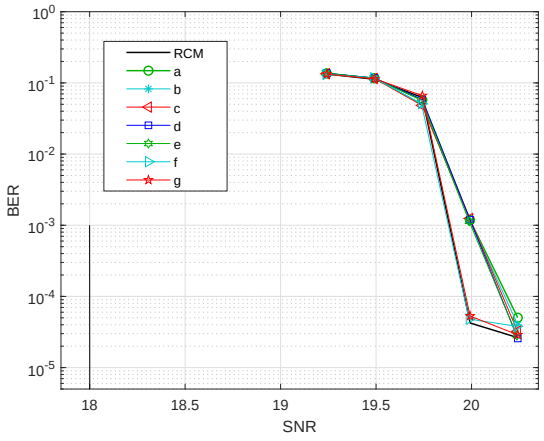

(a) $R = 6$

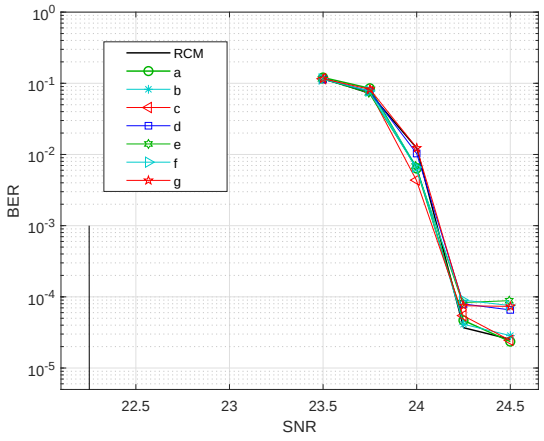

(b) $R = 7.4$

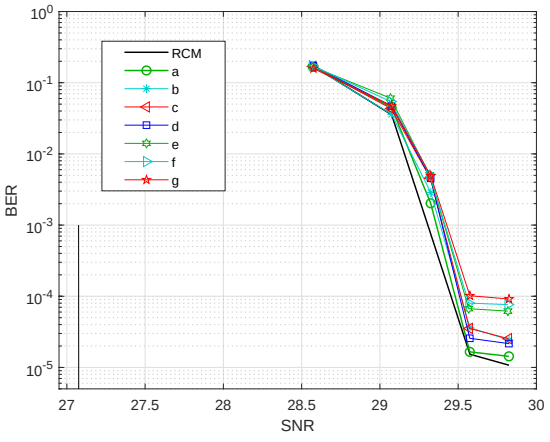

(c) $R = 9$

FIGURE 6: Numerical results obtained by Monte Carlo simulations for the asymmetric multi-user scenario with rate distributions as in Table 1 and for point-to-point (RCM) when the AWGN MAC is considered. The weight sets $\mathcal{W}$ are (a) $\{3, 3, 4, 5\}$ for $R = 6$, (b) $\{3, 4, 5, 7\}$ for $R = 7.4$ and (c) $\{3, 4, 5, 5, 7\}$ for $R = 9$.

total block length is increased according to λ, so that K_l stays fixed when the number of users increases. This is shown in Fig. 7 for the case of $R = 7.4$ with symmetric rate allocation. Figs. 7a, 7b and 7c show the performance when the individual block length of each user K_l, for $l = 1, \ldots, \lambda$, is fixed to 1110, 4440 and 8880, respectively. The coded block length (in complex coded symbols) is given by $\frac{M}{2} = \frac{K}{R}$, where $K = \lambda \cdot K_l$ is the total number of information bits transmitted per block.

Figs. 7a, 7b and 7c show that the performance depends both on the total block length K and the individual block length K_l. For example, in the case of $K_l = 1110$ there is a minimum error floor of around 10^{-4} that is achieved with $\lambda = 16$, (i.e. a total block length $K = 17760$), and the error floor does not improve any further when λ increases. On the other hand, when $K_l = 8880$ and $\lambda = 2$, with the same total block length $K = 17760$, the error floor improves to $6 \cdot 10^{-5}$. As can be seen in Fig. 7c, any number of users can be sent with a low error floor provided that the total and the individual (per user) block lengths are large enough.

C. NUMERICAL RESULTS FOR THE RAYLEIGH FAST FADING MAC

As mentioned in Section II-B, when the number of users increases, the sum-rate capacity of the Rayleigh fast fading MAC increases towards its maximum value, namely the sum-rate capacity of the AWGN MAC. Assuming symmetric rate allocation, Table 2 shows the SNR Shannon limits for $\lambda = 1, 2, 3, 4$ ($\lambda = 1$ equals to point-to-point RCM) and sum-rates R=6, 7.4 and 9. The table also shows the SNR Shanon limit when the number of users grows asymptotically.

TABLE 2: Shannon SNR limits (in dB) for the symmetric rate allocation with sum-rate R in the Rayleigh fast fading MAC.

λ	$R = 6$	$R = 7.4$	$R = 9$
1	20.4	24.7	29.6
2	19.1	23.4	28.3
3	18.7	23	27.8
4	18.6	22.8	27.7
∞	18	22.3	27.1

For the simulations, the weight sets $\mathcal{W}$ have been selected for each λ using the modified EXIT charts detailed in Section IV-D. The optimized weight sets $\mathcal{W}$ are $\{2, 3, 4, 4, 7\}$ for $R = 6$ and $\{3, 4, 5, 8, 10\}$ for $R = 7.4$ and 9, independently of the number of users ($\lambda = 1, \ldots, 128$).

Fig. 8 plots the resulting performance for the symmetric rate scenario, with $\lambda = 2, 3, 4, 8, 16, 32, 64$ and 128, indicated as $\lambda \times 1$ in the figure, and the point-to-point RCM. For the sake of clarity in the figures, only the SNR limits corresponding to a larger number of users (SNR_∞) are plotted as vertical lines, with values given by $\text{SNR}_\infty = 18$ dB, $\text{SNR}_\infty = 22.3$ dB and $\text{SNR}_\infty = 27.1$ dB for $R = 6$, 7.4 and 9, respectively.

Notice that, following the theoretical limits, performance improves as the number of users increases. For example, Fig. 8a shows that for $R = 6$ the MAC scenario with $\lambda = 16$ users requires an SNR of around 0.7 dB less than the system with $\lambda = 2$ users, and 1.15 dB less SNR than the point-to-

This article has been accepted for publication in a future issue of this journal, but has not been fully edited. Content may change prior to final publication. Citation information: DOI 10.1109/ACCESS.2020.3043529, IEEE Access

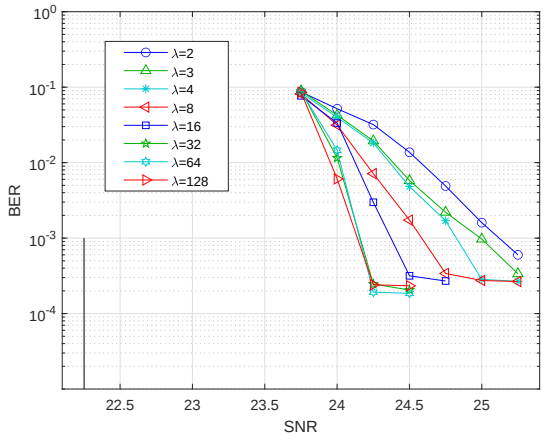

(a) $K_l = 1110$

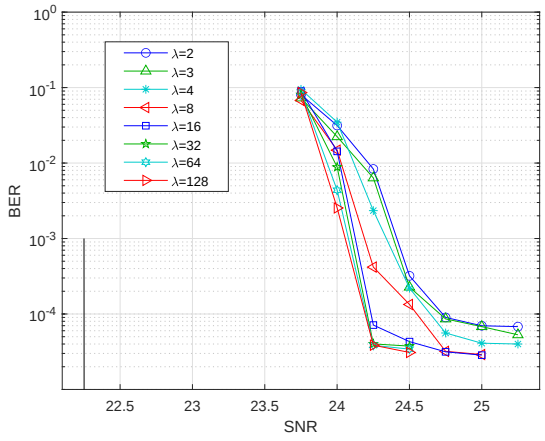

(b) $K_l = 4440$

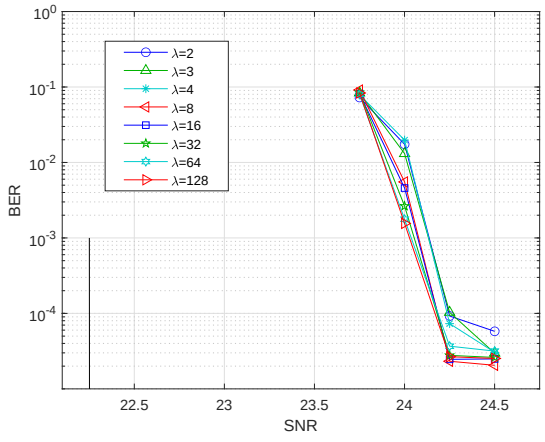

(c) $K_l = 8880$

FIGURE 7: Numerical results obtained by Monte Carlo simulations for the symmetric multi-user scenario of $R = 7.4$ with $\lambda \in \{2, 3, 4, 8, 16, 32, 64, 128\}$ when the AWGN MAC is considered. The weight set is $\{3, 4, 5, 7\}$. The parameter K_l is fixed to (a) 1110, (b) 4440 and (c) 8880. The parameter M is scaled with the number of users to maintain the sum-rate R fixed.

point RCM code, to achieve the same BER. Similarly, we can see in Fig. 8b that for $R = 7.4$ and $\lambda = 16$ users the SNR improvement is around 1.15 dB and 0.65 dB compared to the results of the point-to-point RCM code and to the case with $\lambda = 2$ users, respectively. Finally, results for $R = 9$ are shown in Fig. 8c. In this case, the SNR improvement for $\lambda = 16$ users compared to the point-to-point RCM case is increased to around 2 dB. Notice also that for more than 16 users the performance no longer improves significantly. The reason is that the weight sets have length five, and thus, at each RCM-MAC symbol only the averaging effect of up to 10 users applies.

The results for the asymmetric rate allocation case are showed in Fig. 9, where the same trends as in the symmetric scenario are observed. It is interesting to notice that for all rate allocation scenarios, as in the case of standard point-to-point RCM codes, RCM-MAC codes suffer from error floors of around 10^{-3}. This paves the way for future research on lowering the error floor by concatenating the proposed RCM-MAC to other codes, as has been done for point-to-point RCM codes.

TABLE 3: Summary of the SNR performance improvement (in dB) when comparing the RCM-MAC system with the point-to-point RCM in a Rayleigh fast fading MAC ($\lambda = 1$). Both symmetric and asymmetric rate allocations (refer to Table 1) are included.

	RCM-MAC	$R = 6$	$R = 7.4$	$R = 9$
symmetric	$\lambda = 2$	0.45	0.5	1.3
	$\lambda = 3$	0.76	0.65	1.4
	$\lambda = 4$	0.84	0.87	1.6
	$\lambda = 8$	1.1	1.07	1.67
	$\lambda = 16$	1.15	1.13	1.8
	$\lambda = 32$	1.25	1.2	1.95
	$\lambda = 64$	1.25	1.2	1.95
	$\lambda = 128$	1.25	1.2	1.95
asymmetric	a	0.4	0.53	1.15
	b	0.5	0.57	1.25
	c	0.65	0.73	1.35
	d	0.78	0.77	1.53
	e	0.8	0.87	1.55
	f	0.88	0.95	1.68
	g	0.92	0.97	1.68

To sum up, the SNR performance gap of the RCM-MAC codes with respect to the theoretical limits is around 2 dB in the AWGN case and 2.7-3.5 dB in the Rayleigh fast fading case. These gaps are around 1 dB worse than the ones discussed in [17], where low rates are considered. This is consistent with the performance loss typically observed when comparing high spectral efficiency codes like RCM, Hybrid ARQ or BICM, which operate within 1-2 dBs from the limit [20], with low-rate codes, such as LDPC, which closely approach the Shannon limit [31]. RCM-MAC systems provide larger system throughputs, and accommodate a large number of users without impacting the performance and decoding complexity. Moreover, for Rayleigh fast fading, performance is improved when the number of simultaneous users increases. Table 3 presents the SNR performance improve-

This article has been accepted for publication in a future issue of this journal, but has not been fully edited. Content may change prior to final publication. Citation information: DOI 10.1109/ACCESS.2020.3043529, IEEE Access

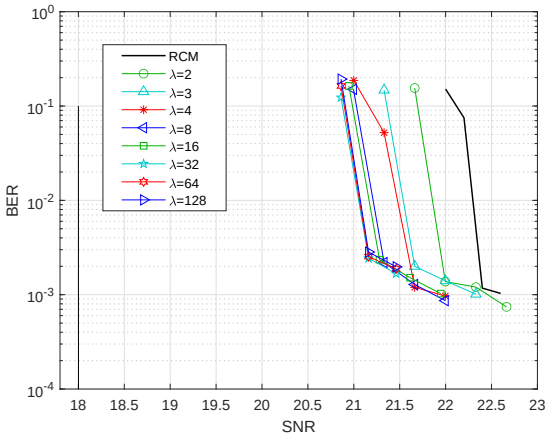

(a) $R = 6$

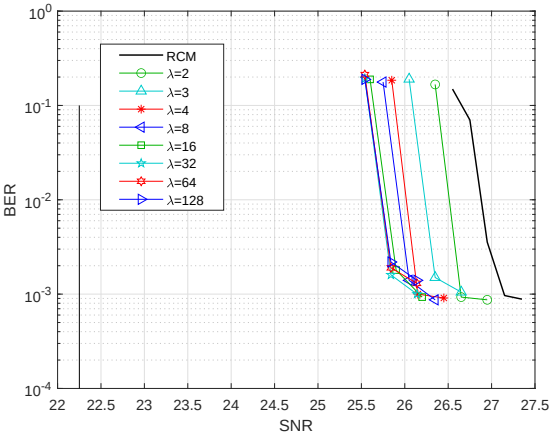

(b) $R = 7.4$

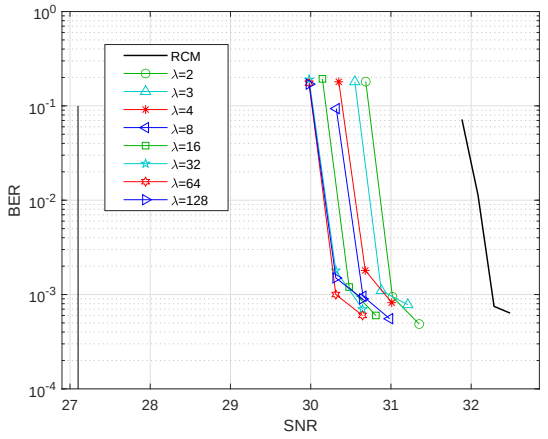

(c) $R = 9$

FIGURE 8: Numerical results obtained by Monte Carlo simulations for the symmetric multi-user scenario with $\lambda \in \{2, 3, 4, 8, 16, 32, 64, 128\}$ and the point-to-point RCM code (denoted by RCM) when a Rayleigh fast fading MAC is considered. The weight sets $\mathcal{W}$ are (a) $\{2, 3, 4, 4, 7\}$ for $R = 6$, (b) $\{3, 4, 5, 8, 10\}$ for $R = 7.4$ and (c) $\{3, 4, 5, 8, 10\}$ for $R = 9$. The asymptotic limits when the number of users increases to infinity have been plotted as reference.

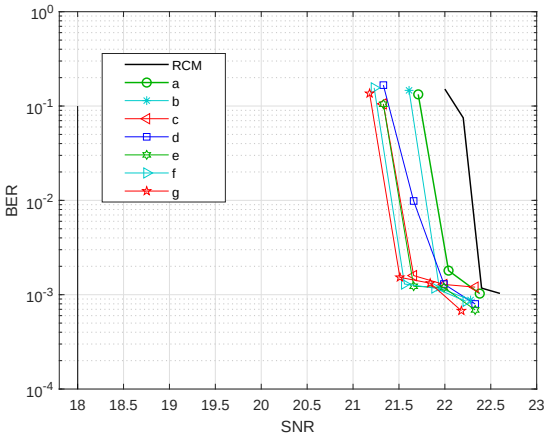

(a) $R = 6$

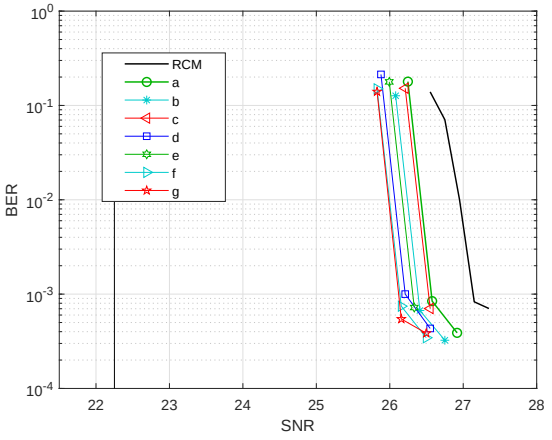

(b) $R = 7.4$

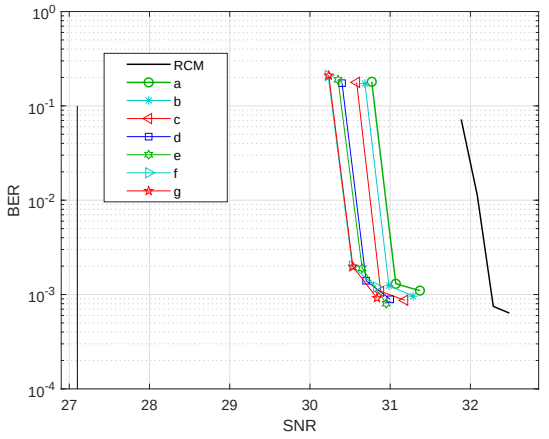

(c) $R = 9$

FIGURE 9: Numerical results obtained by Monte Carlo simulations for the asymmetric multi-user scenario with rate distributions as in Table 1 and the point-to-point RCM code (denoted by RCM) when a Rayleigh fast fading MAC is considered. The weight sets $\mathcal{W}$ are (a) $\{2, 3, 4, 4, 7\}$ for $R = 6$, (b) $\{3, 4, 5, 8, 10\}$ for $R = 7.4$ and (c) $\{3, 4, 5, 8, 10\}$ for $R = 9$. The asymptotic limits when the number of users increases to infinity have been plotted as reference.

ments obtained in the proposed RCM-MAC system when the number of users increases and the channel is Rayleigh fast fading. The entries indicate the SNR improvement (in dB, and for BER $= 10^{-2}$) with respect to the case of 1 user

utilizing a point-to-point RCM code.

VI. CONCLUSIONS

A new high-rate coding scheme for non-orthogonal multiple access has been proposed. The MAC coding scheme is based on the use of irregular RCM codes for each user and is constructed in such a way that the combination of all generation matrices forms a standard point-to-point RCM code but with some extra constraints. At the receiver, the information transmitted from the users is jointly decoded by applying the RCM sum-product algorithm over the factor graph that results from the combination of the individual RCMs. Thus, the decoding complexity of RCM-MAC codes is independent of the number of users. To the extend of the authors' knowledge, the proposed techniques are the first MAC coding schemes that allow to accommodate up to 128 users while operating at high rates and without making use of additional set-ups like multiple antennas.

For the AWGM MAC channel, and for a large range of simultaneous users, simulation results show that the performance of the proposed MAC scheme is around 2 dB away from the Shannon limit. On the other hand, when considering the Rayleigh fast fading channel, the Shannon limit depends on the number of users. The performance of our proposed scheme is around 2.7-3.5 dB away from these limits.

In our future research, we will study how to lower the error floor that appears in RCM-MAC codes, as has been done for point-to-point RCM codes in the literature. Furthermore, we plan to adapt RCM-MAC codes to scenarios where users transmit correlated information, by utilizing the low-density nature of RCM codes to maintain the source correlation in the transmitted codewords.

REFERENCES

[1] N. Jaiswal and N. Purohit, "Performance Evaluation of Non-orthogonal Multiple Access in V2V communications Over Double-Rayleigh Fading Channels," *2019 IEEE Conference on Information and Communication Technology*, Allahabad, India, 2019, pp. 1-5, doi: 10.1109/CICT48419.2019.9066141.

[2] M. B. Janjua, D. B. da Costa and H. Arslan, "User Pairing and Power Allocation Strategies for 3D VLC-NOMA Systems," in *IEEE Wireless Communications Letters*, vol. 9, no. 6, pp. 866-870, June 2020, doi: 10.1109/LWC.2020.2973628.

[3] F. Ghanami, G. A. Hodtani, B. Vucetic and M. Shirvanimoghaddam, "Performance Analysis and Optimization of NOMA with HARQ for Short Packet Communications in Massive IoT," in *IEEE Internet of Things Journal*, doi: 10.1109/JIOT.2020.3028434.

[4] Y. Saito, Y. Kishiyama, A. Benjebbour, T. Nakamura, A. Li, and K.Higuchi, "Non-orthogonal multiple access (noma) for cellular future radio access", in *Proc. Vehicular Technology Conference (VTC Spring) 2013 IEEE 77th*, pp. 1-5, June 2013.

[5] M. Al-Imari, P. Xiao, M. A. Imran, and R. Tafazolli, "Uplink non-orthogonal multiple access for 5g wireless networks", in *Proc. 2014 11th International Symposium on Wireless Communication Systems*, pp. 781-785, August 2014.

[6] N. Otao, Y. Kishiyama, and K. Higuchi, "Performance of non-orthogonal access with SIC in cellular downlink using proportional fair-based resource allocation", in *Wireless Communication Systems (ISWCS), 2012 International Symposium on IEEE*, pp. 476-480, August 2012.

[7] M. Elhattab, M. A. Arfaoui, C. Assi and A. Ghrayeb, "Reconfigurable Intelligent Surface Assisted Coordinated Multipoint in Downlink NOMA Networks," in *IEEE Communications Letters*, doi: 10.1109/LCOMM.2020.3029717.

[8] S. M. R. Islam, N. Avazov, O. A. Dobre and K. Kwak, "Power-Domain Non-Orthogonal Multiple Access (NOMA) in 5G Systems: Potentials and Challenges," in *IEEE Communications Surveys & Tutorials*, vol. 19, no. 2, pp. 721-742, Secondquarter 2017, doi: 10.1109/COMST.2016.2621116.

[9] L. Dai, B. Wang, Y. Yuan, S. Han, C. 1. I, and Z. Wang, "Non-orthogonal multiple access for 5G: solutions, challenges, opportunities, and future research trends", in *IEEE Communications Magazine*, vol. 53, no. 9, pp. 74-81, September 2015.

[10] S. Verdú, "Multiuser Detection". *Cambridge University Press*, 1998.

[11] J. A. de Carvalho, D. B. da Costa, F. R. M. Lima, R. Oliveira and U. S. Dias, "Non-Orthogonal Multiple Access in Two-Hop Wireless Powered Communication Networks," in *IEEE Wireless Communications Letters*, vol. 9, no. 9, pp. 1398-1402, Sept. 2020, doi: 10.1109/LWC.2020.2992049.

[12] J. A. de Carvalho, D. B. da Costa, L. Yang, G. C. Alexandropoulos, R. Oliveira and U. S. Dias, "User Fairness in Wireless Powered Communication Networks with Non-Orthogonal Multiple Access," in *IEEE Wireless Communications Letters*, doi: 10.1109/LWC.2020.3030818.

[13] K. Chung, "NOMA for Correlated Information Sources in 5G Systems," in *IEEE Communications Letters*, doi: 10.1109/LCOMM.2020.3027726.

[14] H. Pan, L. Lu, and, S. C. Liew, "Practical Power-Balanced Non-Orthogonal Multiple Access", in *IEEE Journal on Selected Areas in Communications*, vol. 35, no. 10, pp. 2312-2327, October 2017.

[15] Y. Zhang, K. Peng, S. Chen, and J. Song, "A capacity-approaching multi-user BICM-ID scheme for multiple access channel, in *2015 International Wireless Communications and Mobile Computing Conference (IWCMC)*, August 2015.

[16] Li Ping, Lihai Liu, Keying Wu and W. K. Leung, "Interleave division multiple-access," in *IEEE Transactions on Wireless Communications*, vol. 5, no. 4, pp. 938-947,

April 2006, doi: 10.1109/TWC.2006.1618943.

[17] M. Gonzalez-Lopez, F. J. Vazquez-Araujo, L. Castedo and J. Garcia-Frias, "Interleave-division multiple access (IDMA) using low-rate layered LDGM codes," 2008 5th International Symposium on Turbo Codes and Related Topics, Lausanne, 2008, pp. 315-320, doi: 10.1109/TURBOCODING.2008.4658718.

[18] Y. Chen, J. Schaepperle and T. Wild, "Comparing IDMA and NOMA with superimposed pilots based channel estimation in uplink," *2015 IEEE 26th Annual International Symposium on Personal, Indoor, and Mobile Radio Communications (PIMRC)*, Hong Kong, 2015, pp. 89-94, doi: 10.1109/PIMRC.2015.7343274.

[19] H. Cui, C. Luo, K. Tan, F. Wu and C. W. Chen, "Seamless rate adaptation for wireless networking", in *Proc. 2011 ACM MSWiM*, pp. 437-446, October 2011.

[20] H. Cui, C. Luo, J. Wu, C. W. Chen and F. Wu, "Compressive Coded Modulation for Seamless Rate Adaption", *IEEE Trans. on Wireless Communications*, pp. 4892-4904, October 2013.

[21] F. Lu, Y. Dong, W. Rao and C. W. Chen, "Low Complexity Decoding Algorithms for Rate Compatible Modulation," in *IEEE Access*, vol. 6, pp. 31417-31429, 2018, doi: 10.1109/ACCESS.2018.2842095.

[22] L. Li, J. Garcia-Frias, "Hybrid Analog Digital Coding Scheme Based on Parallel Concatenation of Liner Random Projections and LDGM Codes", *Proceedings of the 2014 48th Annual Conference on Information Sciences and Systems (CISS)*, Princeton, NJ, USA, 19–21 March 2014.

[23] L. Li, J. Garcia-Frias, "Hybrid Analog-Digital Coding for Nonuniform Memoryless Sources", *Proceedings of the 2015 49th Annual Conference on Information Sciences and Systems (CISS)*, Baltimore, MD, USA, 18–20 March 2015.

[24] I. Granada, P.M. Crepo, J. Garcia-Frias, "Asymptotic BER EXIT chart analysis for high rate codes based on the parallel concatenation of analog RCM and digital LDGM codes" *J. Wireless Communication and Networks:* 2019, *11*.

[25] I. Granada, P.M. Crepo, J. Garcia-Frias, "Combining the Burrows-Wheeler Transform and RCM-LDGM Codes for the Transmission of Sources with Memory at High Spectral Efficiencies", *Entropy* 2019, *21(4)*.

[26] A. El Gamal, Y.-H. Kim, "Network Information Theory" *Cambridge University Press*, 2012.

[27] F.R. Kschischang, B.J. Frey, H.-A. Loeliger, "Factor Graphs and the Sum-Product Algorithm", *IEEE Trans. Inf. Theory* 2001, *47*, 498–519.

[28] S. ten Brink, "Convergence of iterative decoding," in *Electronics Letters*, vol. 35, no. 10, pp. 806-808, 13 May 1999, doi: 10.1049/el:19990555

[29] S. ten Brink, G. Kramer and A. Ashikhmin, "Design of low-density parity-check codes for modulation and detection," in *IEEE Transactions on Communications*, vol. 52, no. 4, pp. 670-678, April 2004, doi: 10.1109/TCOMM.2004.826370.

[30] S. R. Kollu and H. Jafarkhani, "On the EXIT chart analysis of low-density parity-check codes," *GLOBECOM '05. IEEE Global Telecommunications Conference, 2005.*, St. Louis, MO, 2005, pp. 6 pp.-, doi: 10.1109/GLOCOM.2005.1577830.

[31] Sae-Young Chung, G. D. Forney, T. J. Richardson and R. Urbanke, "On the design of low-density parity-check codes within 0.0045 dB of the Shannon limit," in *IEEE Communications Letters*, vol. 5, no. 2, pp. 58-60, Feb 2001, doi: 10.1109/4234.905935.

IMANOL GRANADA received the B.S. (Distinction) and M.S. degrees in telecommunications engineering from the TECNUN - School of Engineering (University of Navarra), San Sebastián, Spain, in 2015 and 2017, respecetively. He is currently pursuing the Ph.D. degree in telecommunications engineering as a research assistant within the Basic Sciences and Mathematics Group at the TECNUN - School of Engineering in San Sebastián.

His research interests are in the area of wireless communications and networks with special focus on adaptive coded modulation, joint source-channel coding and multiple access channels.

PEDRO M. CRESPO received the engineering degree in Telecommunications from Universidad Politćnica de Cataluña, Barcelona, Spain in 1987, and the M. Sc. in applied Mathematics and Ph.D. in Electrical Engineering from University of Southern California, CA, USA, in 1983 and 1984, respectively. From September 1984 to April 1992, he was a member of the technical staff at the Signal Processing Research group in Bell Communications Research, NJ, USA, where he worked in the areas of data communication and signal processing. He actively contributed in the definition and development of the first prototypes of xDSL (Digital Subscriber Lines transceivers). From May 1992 to August 1999 he was a district manager at Telefónica R&D, Madrid, Spain. From 1999 to 2002 he was the technical director of the Spanish telecommunication operator Jazztel. Latter and until 2009 he became director of the Electronics and Communication department at the R&D center CEIT (www.ceit.es), San Sebastián, Spain. At present, he is a Professor at TECNUN-School of Engineering, University of Navarra, San Sebastián, Spain.

His research interests are in the area of information and signal processing with a focus on wireless communications and networks. More recently, his interests also include quantum information theory and coding.

Pedro M. Crespo is a Senior Member of the Institute of Electrical and Electronic Engineers (IEEE) and he is a Recipient of Bell Communication Research's Award of excellence. Dr. Crespo holds seven patents in the areas of digital subscriber lines and wireless communications.

JAVIER GARCIA-FRÍAS (S'93–M'99–SM'08) received the Ingeniero de Telecomunicación degree from the Universidad Politécnica de Madrid, Spain, in 1992, the Licenciado en Ciencias Matemáticas degree from UNED, Madrid, in 1995, and the Ph.D. degree in electrical engineering from UCLA, in 1999. In 1992, and from 1994 to 1996, he was with Telefónica I+D, Madrid. From 1999 to 2008, he was an Assistant and then an Associate Professor with the Department of Electrical and Computer Engineering, University of Delaware, where he is currently a Professor.

His research interests are in the area of information processing in communications and biological systems, with a focus on wireless communications, iterative decoding schemes for source and channel coding, coding for multiterminal sources, joint source-channel coding, analog coding, quantum error correcting codes, and probabilistic techniques in biological systems. He has been a member of the Signal Processing for Communications Technical Committee in the IEEE Signal Processing Society from 2004 to 2006.

He was a recipient of a 2001 NSF CAREER Award and a 2001 Presidential Early Career Award in support of his communications program. He has served as an Editor and a Guest Editor of several journals, including the *IEEE Signal Processing Magazine* in 2007, the *IEEE TRANSACTIONS ON WIRELESS COMMUNICATIONS* from 2003 to 2007, the *IEEE TRANSACTIONS ON SIGNAL PROCESSING* from 2004 to 2006, and the *EURASIP Journal on Bioinformatics and Systems Biology* from 2005 to 2014.